Pretargeted Immuno-PET Enables Monoclonal Antibody Imaging Beyond the Blood-Brain Barrier

Gustavsson, Tobias; Kustermann, Thomas; Hvass, Lars; Wuensche, Thomas E.; Clausen, Anne Skovsbo; Stotz, Sophie; Shalgunov, Vladimir; van den Broek, Sara Lopes; Knudsen, Gitte M.; Aldana, Blanca; Ferri, Elena; Cannazza, Giuseppe; Niewoehner, Jens; Gobbi, Luca; Honer, Michael; Battisti, Umberto Maria; Kjaer, Andreas; Herth, Matthias M.

Published in:
Molecular Pharmaceutics

DOI:
10.1021/acs.molpharmaceut.5c01180

Publication date:
2025

Document version
Publisher's PDF, also known as Version of record

molecular pharmaceutics

pubs.acs.org/molecularpharmaceutics

Article

Pretargeted Immuno-PET Enables Monoclonal Antibody Imaging Beyond the Blood–Brain Barrier

Published as part of Molecular Pharmaceutics special issue "Innovations in Nuclear Medicine".

Tobias Gustavsson, Thomas Kustermann, Lars Hvass, Thomas E. Wuensche, Anne Skovsbo Clausen, Sophie Stotz, Vladimir Shalgunov, Sara Lopes van den Broek, Gitte M. Knudsen, Blanca Aldana, Elena Ferri, Giuseppe Cannazza, Jens Niewoehner, Luca Gobbi, Michael Honer, Umberto Maria Battisti,* Andreas Kjaer,* and Matthias M. Herth*

Cite This: *Mol. Pharmaceutics* 2025, 22, 7600–7610

Read Online

ACCESS | Metrics & More | Article Recommendations | Supporting Information

ABSTRACT: Pretargeted PET imaging offers a powerful approach to improve nuclear imaging contrast and reduce systemic radiation exposure, yet its application in the brain has been limited by the blood–brain barrier (BBB). Here, we demonstrate, for the first time, successful pretargeted PET imaging of a brain target enabled by a bispecific antibody engineered for transferrin receptor-mediated BBB transcytosis. By combining this brain shuttle with a novel ^{18}F-labeled tetrazine, we achieve specific, quantifiable detection of brain-localized Aβ aggregates, validated through PET imaging and histological analysis. This proof-of-concept establishes a versatile, noninvasive imaging platform with broad potential for assessing biologic drug candidates and CNS targets previously considered intractable.

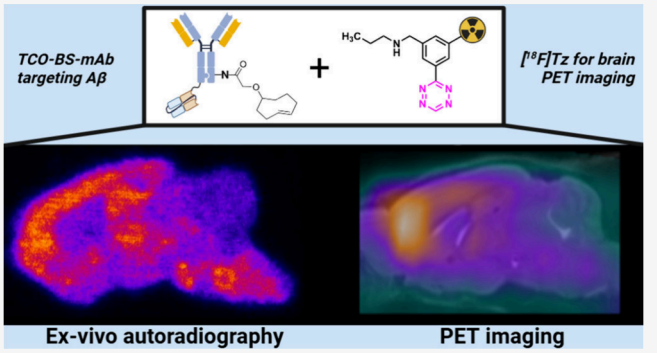

KEYWORDS: *pretargeting, Imaging CNS, blood–brain barrier, transferrin receptor, tetrazine ligation*

INTRODUCTION

Drug development for many neurodegenerative diseases, such as Alzheimer's disease (AD) or Parkinson's disease (PD), has proven complex over the past decades. A major obstacle to progress is the blood–brain barrier (BBB), which limits brain exposure of the drug.[1] Another challenge in CNS drug development is demonstrating target engagement or impact on disease progression. This is partly due to the lack of suitable positron emission tomography (PET) tracers. Amyloid beta (Aβ), tau, or α-synuclein (α-syn), and their various oligomeric, protofibril, and (iso)forms are the pathological hallmarks of AD and PD and remain some of the primary therapeutic targets in the development of treatment interventions. While there are validated PET tracers for proteins such as aggregated Aβ and 3R/4R tau,[2,3] the relative sensitivity for structurally different pathological species (e.g., oligomers, protofibrils, and fibrils) remains unknown. For other targets, such as aggregated forms of α-syn or TDP-43, no suitable PET tracers exist. Increasing focus on other pathogenic factors like neuroinflammation, mitochondrial dysfunction, or synaptic dysfunction has highlighted the need to develop tracers for other proteins, particularly for those considered "undruggable", i.e., for proteins where small molecule PET tracer discovery has been challenging. High molecular weight binders such as monoclonal antibodies (mAbs) offer significant advantages for CNS imaging due to their excellent target specificity and availability for numerous targets. This addresses a key limitation of small molecule PET tracers in many CNS applications. Despite these advantages, their size severely restricts their ability to permeate the BBB in high concentrations, thereby limiting overall brain uptake. Recent advances have shown promise in overcoming this challenge. Modification of large molecules with a BBB-targeting moiety, such as the Brainshuttle technology, can significantly improve brain penetration, with reported increases of up to 100-fold,[4] e.g., by conjugation with a transferrin receptor targeting moiety, offer an alternative imaging approach.[5−10] This approach bears the opportunity to repurpose existing libraries of antibody constructs for PET imaging, thereby considerably reducing the need for de novo PET tracer discovery programs.

Received: August 13, 2025
Revised: September 25, 2025
Accepted: September 26, 2025
Published: November 6, 2025

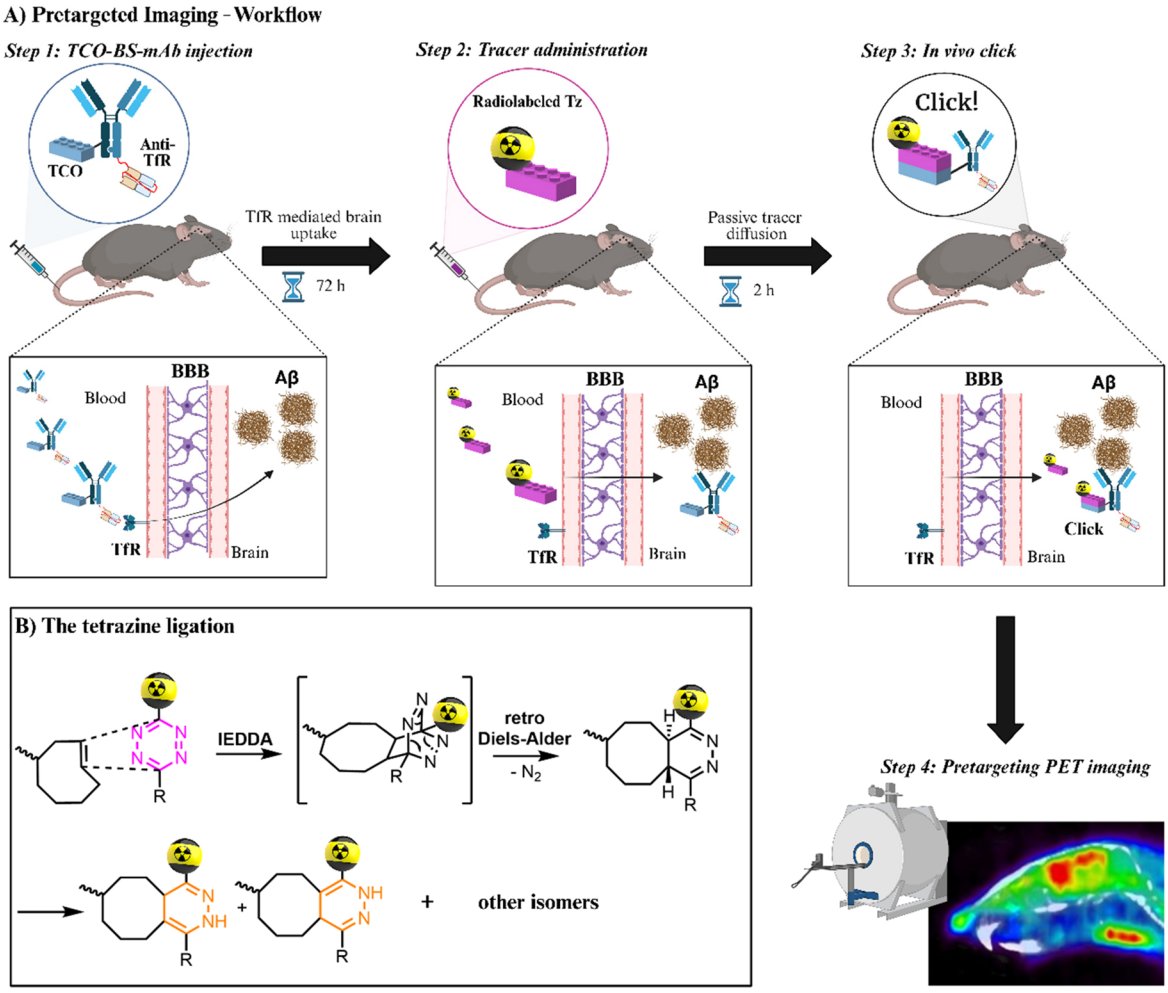

Figure 1. Overview of the pretargeted PET imaging strategy used in this study. (A) Schematic representation of the pretargeting workflow for imaging Aβ pathology beyond the BBB. A two-step approach was employed: first, the pretargeting vector **TCO-BS-mAb31** was administered systemically, allowing time (72 h) for accumulation of Aβ plaques and clearance from circulation. Subsequently, the radiolabeled imaging agent [^{18}F]**1** was injected and selectively bound to the vector via bioorthogonal ligation. (B) The ligation chemistry is based on the inverse electron-demand Diels–Alder reaction between *trans*-cyclooctene (TCO) and tetrazine (Tz), enabling rapid and selective *in vivo* labeling.

Recent preclinical studies have shown that antibody-based PET imaging is feasible for targets beyond the BBB.[7,10−12] However, the slow tissue distribution and clearance of mAbs necessitate radionuclides with long decay half-lives to achieve adequate signal-to-background ratios for PET imaging. Typically, these radionuclides also result in a high radiation burden to patients.[6,8,13−15]

In contrast, pretargeting allows PET imaging with antibodies using short-lived radionuclides (i.e., ^{18}F and ^{11}C). This is achieved by uncoupling the typically long biological half-life of antibodies from the radionuclide decay half-life, which lowers the radiation burden while providing the imaging contrast of small molecule PET tracers combined with the exquisite affinity and specificity of mAbs.[14] Several pretargeting strategies are based on bioorthogonal reactions.[15−18] The most prominent bioorthogonal reaction is the tetrazine ligation between a *trans*-cyclooctene (TCO) and a tetrazine (Tz) (Figure 1B). This ligation is highly selective, ultrafast (up to 10^{7-9} M^{-1} s^{-1}), irreversible, and results in a stable product.[19]

While several examples of pretargeted tumor imaging in the periphery have been reported,[17] successful application of pretargeted imaging in the brain remains elusive, except where targeted vectors have been directly administered via intrathecal or intracerebral routes.[18,20−24] While these studies provided valuable proof-of-principle, the concentrated and highly localized target is not physiologically representative and does not reflect a realistic *in vivo* scenario. Roche developed the Brainshuttle (BS) module. which allows for facilitated transport of mAbs across the BBB using transferrin-mediated transcytosis. Here, we use Roche's bispecific antibody (BS-mAb) targeting Aβ. Concurrently, we developed an ^{18}F-labeled Tz that successfully imaged an intracerebral deposited TCO-polymer *in vivo*.[21] The Tz displayed optimal properties for pretargeted brain imaging with high brain uptake and target accumulation, as well as fast blood and brain clearance of unclicked Tz.

In this study, we report for the first time that pretargeted imaging of an intravenously injected TCO-tagged BS-antibody is possible by combining with a BBB penetrant ^{18}F-labeled Tz (Figure 1A). Demonstrating proof-of-principle could enable the broader use of this technology for assessing target engagement and monitoring treatment progress with future therapeutic antibodies.

https://doi.org/10.1021/acs.molpharmaceut.5c01180
Mol. Pharmaceutics 2025, 22, 7600−7610

Table 1. Dosing Information for Mice Pretargeted PET Imaging Using PET/CT (Groups A and B) or PET/MR Systems (Groups 1−5)[a]

	group	pretargeting vector	mAb dose [mg/kg]	genotype	age [months]	n	tracer	injected activity [MBq/g]	injected dose [pmol/g][b]	modality
pilot	**A**	BS-mAb	8.61 ± 0.48	5xFAD	5.5	2	[^{18}F]**1**	0.35 ± 0.06	3.72 ± 0.09	PET/CT
	B	BS-mAb	7.75 ± 0.16	WT	5.5	2	[^{18}F]**1**	0.30 ± 0.03	3.14 ± 0.28	PET/CT
Validation Study	**1**	BS-mAb	8.03 ± 0.47	5xFAD	7.5	6	[^{18}F]**1**	0.48 ± 0.06	7.60 ± 1.20	PET/MR
	2	BS-mAb	7.30 ± 0.48	WT	7.5	3	[^{18}F]**1**	0.46 ± 0.04	34.33 ± 2.87	PET/MR
	3	BS-iso	8.40 ± 0.37	5xFAD	7.5	3	[^{18}F]**1**	0.45 ± 0.05	30.07 ± 0.71	PET/MR
	4			5xFAD	7.5	3	[^{18}F]**1**	0.52 ± 0.07	23.46 ± 1.72	PET/MR
	5	BS-mAb	7.67 ± 0.47	5xFAD	7.5	3	[^{18}F]**2**	0.49 ± 0.05	5.97 ± 0.58	PET/MR

[a]Values are presented as the mean ± standard deviation. [b]Doses were calculated based on end-of-synthesis results. Groups A−B represent the first cohort; groups 1−5 represent the second cohort.

METHODS

TCO-Functionalization of Antibodies. Roche provided the 200 kDa bispecific antibody constructs BS-mAb and BS-iso. TCO functionalization was performed using axial NHS-TCO under the following conditions: 1−1.5 mg (5−7.5 nmol) of mAb reacted with a 5:1, 10:1, and 20:1 molar ratio of NHS-TCO to mAb in 300−500 μL of 1× phosphate-buffered saline (PBS) at pH 8.4−8.5. The conjugation reaction was carried out in the dark under agitation of 500 rpm at room temperature for 3 h. Unreacted NHS-TCO was removed with Zeba spin desalting columns, 7K MWCO (Thermofisher, 89890) according to the manufacturer's instructions, and eluted in sterile 0.22 μm filtered PBS. The concentration of isolated TCO-mAbs were determined using a NanoDrop spectrophotometer and stored at −80 °C until further use. Determination of active TCO-load was done as previously described and detailed information is given in the Supporting Information (SI).[21]

Postlabeling *in Vitro* Assays. *Analytical Size-Exclusion Chromatography.* Antibody integrity following TCO-functionalization was assessed via size-exclusion high-performance liquid chromatography (Ultimate 3000 system, Thermofisher) using a Superdex 200 Increase 10/300 GL (Cytiva) with saline phosphate buffer, pH 6.5−7 as mobile phase running at 0.75 mL/min mAb aggregation and fragmentation were evaluated by comparing the area under the curve of the monomer peak (eluting at 14 min) relative to high molecular weight aggregates and fragments in TCO-functionalized mAbs versus unmodified mAbs.

Binding ELISA. The antigen-binding affinity of TCO-modified mAbs was evaluated by using an indirect ELISA assay. Synthetic Aβ_{1-42} peptide (abcam, ab120301) was aggregated as previously described.[9] A 96-well high-binding plate (Corning) was coated with either 2 μg/mL mTfR1 (Nordic biosite, 32-9337-50) or 100 nM aggregated Aβ_{1-42} in PBS and incubated at 4 °C overnight. The following day, blocking was performed with an ELISA blocking buffer (PBS, 1% BSA) for 2 h at room temperature. A serial dilution of unmodified BS-mAb and TCO-BS-mAb, starting at 100 nM with 6-fold dilution steps, was prepared and incubated in ELISA buffer (PBS, 0.1% BSA, 0.05% Tween-20) for 3 h at room temperature. Subsequently, peroxidase-conjugated goat antihuman IgG secondary antibody (0.4 μg/mL, abcam, ab6858) was added and incubated at room temperature for 1 h. The ELISA was developed using TMB substrate solution (ThermoFisher, 34028) and stopped with 2 M HCl, and the absorbance was measured at 450 nm using a microplate reader.

On-Tissue Click Autoradiography. Eight-month-old transgenic 5xFAD mice (n = 2) and age-matched WT mice (n = 2) were intravenously (IV) injected with TCO-BS-mAb at a dose of 8 mg/kg. After 3 days, brains were extracted and immediately frozen at −80 °C. Mouse brains were sectioned using a cryotome under low-light conditions into 20 μm sagittal sections. Prior to on-tissue click autoradiography, brain sections were acclimated to room temperature (RT) for 30 min, followed by a 10 min PBS wash. Subsequently, [^{18}F]**1** was diluted in PBS and applied to the sections at concentration of 20, 1, and 0.33 nM diluted in PBS and incubated in RT under gentle agitation for 60 min. For blocking experiment, tissue sections were preincubated with 20 μM DOTA-Tz for 45 min, followed by 3 × 5 min in PBS washes before the application of 20 nM [^{18}F]**1**. Following [^{18}F]**1** incubation, sections were washed in PBS 3 × 5 min and 30 s in Milli-Q water and air-dried. All procedures were performed under low light conditions. A standard (40, 20, 6.67, 2.22, 0.74, 0.25, 0.08, and 0.03 nM) was prepared from the same [^{18}F]**1** stock solution. Brain tissue sections and [^{18}F]**1** standard were exposed to a phosphor storage screen for 1−24 h and read at 600 dpi using a Cyclone Storage Phosphor system (PerkinElmer Inc.). Regions of interest (ROIs) including the cortex, thalamus, and cerebellum were delineated in Optiquant software (version 3.00, Packard Instruments Co, SI, Figure S7). Based on the [^{18}F]**1** standard curve, regional [^{18}F]**1** concentrations were quantified, and cortex-to-cerebellum and thalamus-to-cerebellum ratios were calculated (SI, Figure S6).

PET Imaging and *ex Vivo* Evaluation. *PET/CT Pilot Study.* Five and a half month old transgenic 5xFAD mice (n = 2) and age-matched WT mice (n = 2) were injected IV with TCO-BS-mAb (dose: ∼8 mg/kg, averaging ∼10 active TCOs/mAb). After 3 days, mice were anesthetized with sevoflurane (4%) and placed in a preheated bed of the preclinical PET/CT scanner (Siemens Medical Solutions). At the start of PET acquisition, 5xFAD mice received 8.7 ± 1.6 MBq of [^{18}F]**1**, while WT mice received 8.6 ± 1.1 MBq. The PET scan lasted 90 min and was followed by a computed tomography (CT) acquisition. Maintenance dose throughout the PET scan was 3% sevoflurane in 30% oxygen enriched air. CT attenuation scans were reconstructed using the Feldkamp algorithm with 2× downsampling. PET list-mode data were binned into time windows of 60 × 10, 10 × 60, 8 × 300, and 3 × 600 s, allowing visualization of tracer uptake and clearance from the brain. Subsequently, PET data were reconstructed using the OSEM3D-MAP algorithm with scatter and attenuation correction. All acquisitions and reconstructions were carried out in the Inveon Research Workplace. Immediately after

https://doi.org/10.1021/acs.molpharmaceut.5c01180
Mol. Pharmaceutics 2025, 22, 7600−7610

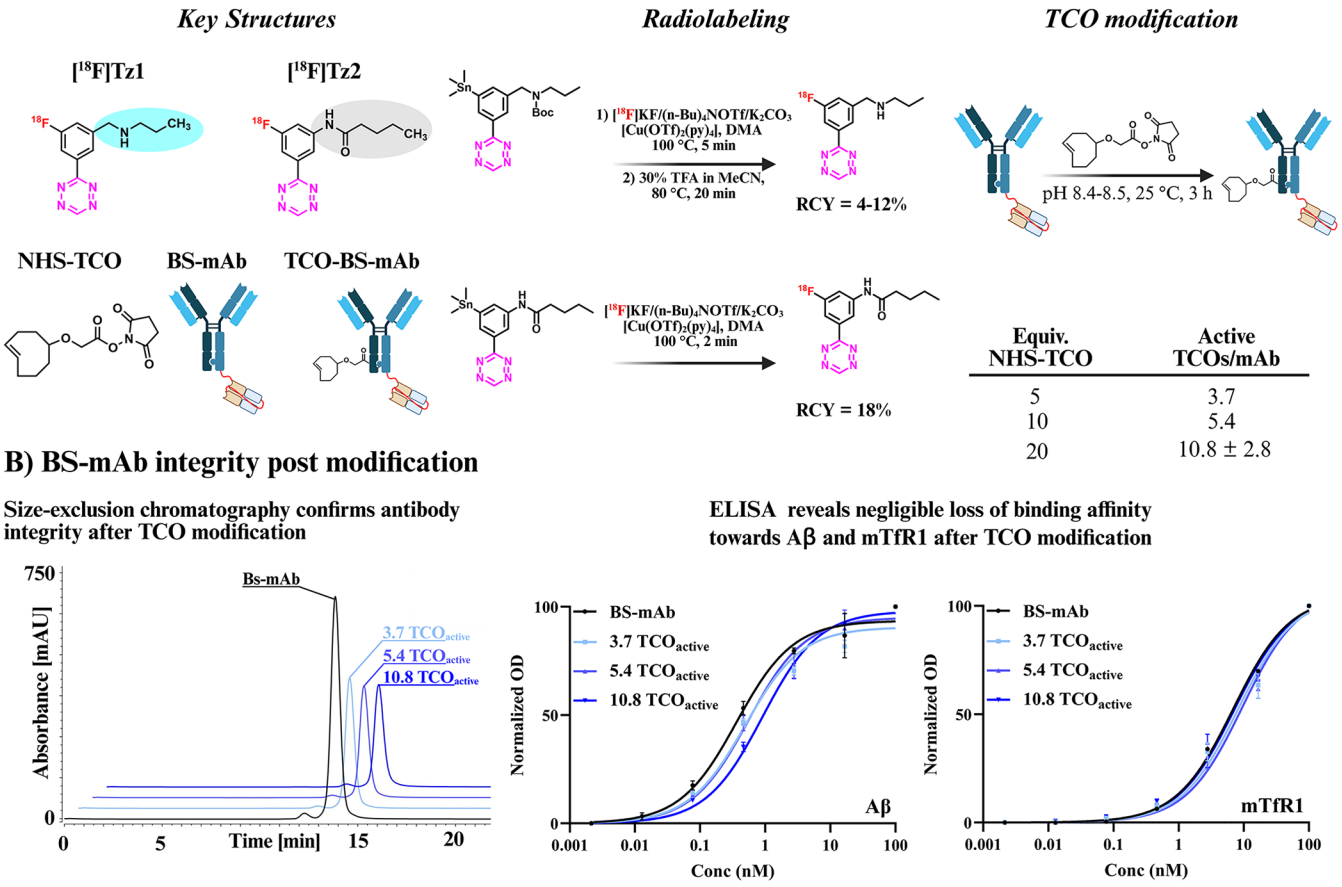

Figure 2. Chemistry and postlabeling assessment of antibody integrity. (A) Key chemicals structures (left), ^{18}F-radiolabeling of both Tzs (middle),[21,27] TCO-antibody modification (right). (B) Size-exclusion chromatography trace of unmodified BS-mAb and TCO-functionalized BS-mAb (left), binding ELISA of BS-mAb and TCO-BS-mAb against Aβ and mTfR1 (right). Values represent mean, and error bar is standard deviation (n = 2).

scanning, mice were euthanized by decapitation, and blood and brain tissues were extracted and weighed.

Processing of PET data was performed in PMOD version 3.910 (PMOD Technologies, Zürich, Switzerland). A standard mouse MRI atlas from Mirrione et al. was used to extract time−activity curves (TACs) from cortical, hippocampal, and cerebellar volumes of interest (VOIs).[25] Representative PET images were created in PMOD by averaging the 60−90 min time frames and coregister them with a mouse brain MRI template from Presotto et al.[26] For representative TACs, since there was a 2 min delay in tracer injection between all mice, linear interpolation was performed to convert all TACs to a common time frame and compensate for variability in intravenous injection timing.

PET/MR Confirmation Follow-up Study. Transgenic 5xFAD mice (n = 14) aged 7.5 months and aged-matched WT mice (n = 3) were included in a follow-up study. The mice were injected IV with TCO-functionalized BS-mAb or BS-iso (averaging ∼10 active TCOs/mAb, detailed dosing information in Table 1) or tracer injection without prior TCO-mAb administration. After 3 days, mice were anesthetized with 4% sevoflurane and injected IV with [^{18}F]**1** or [^{18}F]**2**. After 10 min, mice were placed in a preclinical PET/MRI scanner (MR solutions) and scanned for 90 min. Maintenance dose throughout the PET scan was 3% of sevoflurane in 30% oxygen enriched air. During the PET scan, a 3D FLASH MRI scan was obtained for attenuation and scatter correction during PET reconstruction. T1-weighted coronal and axial images were obtained for anatomical reference. Immediately following dynamic PET scan acquisition, mice were euthanized by decapitation, and blood, brain, and peripheral organs were resected and weighed. PET list-mode data were binned into sequential time windows of 20 × 30 s, 10 × 60 s, 8 × 300 s, and 3 × 600 s and reconstructed using OSEM3D algorithm using 4 iterations and 16 subsets with scatter and attenuation correction. Processing of PET/MR data was performed in the same manner as for PET/CT, using PMOD version 3.910 (PMOD Technologies, Zürich, Switzerland). A standard mouse MRI atlas was used to extract SUV TACs from cortical, hippocampal, and cerebellar VOIs. Tracer uptake in the brain was quantified as SUV in the 80−90 min time frame in the selected VOIs. Tracer uptake was plotted in a region-specific manner or as a ratio of the cortex-to-cerebellum or hippocampus-to-cerebellum ratios. Representative images of all experimental groups are given in the (SI, Figure S8).

Post-Mortem Tissue Processing and ex Vivo Analysis. Extracted brains were separated in the symmetrical midline, where one hemisphere was immediately frozen, and the other was further divided into cerebrum and cerebellum parts. The frozen hemisphere was sectioned using a cryotome into 20 μm sagittal sections. Tracer uptake and distribution was examined by *ex vivo* autoradiography. Brain sections were exposed to a

https://doi.org/10.1021/acs.molpharmaceut.5c01180
Mol. Pharmaceutics 2025, 22, 7600−7610

phosphor imaging screen overnight and read at 10 μm resolution with an Amersham Typhoon imager (GE Healthcare). Brain autoradiograms were created in Fiji (v 2.16.0) by converting monochrome data into color image using the fire lookup table and representative images of all groups are given in the SI (Figure S9).

Tissue uptake of [^{18}F]**1** and [^{18}F]**2** was quantified *ex vivo* by gamma counting, and detailed information is given in the SI (Figure S10 and Table S2). Radioactivity in cerebrum, cerebellum, blood, and peripheral organs (lung, liver, heart, spleen, kidney, skull bone, femur bone, muscle, stomach, and small intestine) and radioactive standards was determined by using a Hidex AMG automatic gamma counter (Hidex). Radioactive standards were used to convert counts to Bq and tissue radioactivity was decay corrected to the injection time. Tissue uptake was quantified as *ex vivo* SUV according to formula:

$$\mathrm{SUV}_{exvivo} = \frac{\text{injected activity per gram tissue}}{\text{injected activity per gram body weight}}$$

Immunohistochemistry. The experiments were based on the procedure of Wuensche et al. with slight modifications.[8] Sagittal sections were fixed in cold acetone (approximately −15 °C) for 10 min, quickly dried under an airflow, and blocked with 2% BSA in PBS for 2 h at room temperature (RT). The blocking solution was disposed, and the tissues were incubated with an Alexa Fluor 568 Goat antihuman IgG [H+L] cross-adsorbed secondary HRP-antibody (Invitrogen; 0.4 μg/mL, 1:2000) at RT for 1 h under dark conditions. The antibody solution was disposed, and the tissue was washed 5 times with PBS for 3 min each, followed by a final wash step with deionized water (dH_2O) for 5 min. Subsequently, the tissue was incubated with a 0.5% freshly filtered thioflavin S solution at RT for 8 min under dark conditions. After disposing of the Thioflavin S solution, the tissue was washed for 3 min each in the following order: 2 × 80% EtOH, 1 × 90% EtOH, 3× dH_2O. The tissues were mounted with ProLong Gold Antifade Mountant (Invitrogen, P36930). Images of the stained sections were taken with a fluorescence microscope (ZeissAxio Observer with a Colibri 7 LED light source and an Axiocam 506 monochrome camera) and equally processed using Zen Blue software, version 3.4.91.0.

Statistics. Statistical analysis was performed with the Brown−Forsythe and Welch ANOVA multiple comparison test. A normal Gaussian distribution of the values and no equal variances between groups were assumed. In addition, a Dunnet's T3 correction for multiple comparisons was performed. Significance levels were calculated, and $p < 0.05$ was considered to be statistically significant. All statistical analysis and graphs were generated using GraphPad Prism 10.4.1 software.

RESULTS AND DISCUSSION

Successful Radiolabeling of Our Pretargeted Imaging Agent. Our group has previously synthesized and evaluated several Tzs suitable for pretargeted imaging beyond the BBB.[21,23] From our Tz library, Tzs **1** and **2** (Figure 2A), exhibited particularly favorable physiochemical properties and *in vivo* characteristics (SI, Table S1). Both structures displayed rapid brain uptake, efficient *in vivo* ligation to intracerebral administered TCO-modified polymers and good target-to-background ratios by PET imaging, whereas unreacted Tz cleared rapidly the brain.[21,23] Accordingly, we decided to evaluate these Tz structures as our primary candidate pretargeted imaging agents for this study. Fluorination was performed as previously published.[21,27] The copper-mediated ^{18}F-fluorination resulted in a radiochemical yield (RCY) of approximately 5−12% and 18%, molar activities (A_m) in a range of 13−95 GBq/μmol (time of injection) and a radiochemical purity (RCP) of >90%. A decrease in molar activity of our ^{18}F-labeled tracers was observed after the pilot study, but despite systematic evaluation, no single cause was identified, and experiments were continued due to the aging of the 5xFAD mice; importantly, the issue has not recurred in ongoing studies. Analysis of SUV ratios (cortex-to-cerebellum) versus injected Tz **1** dose in the TCO-BsGant2-5xFAD mouse group showed no correlation between molar activity and imaging contrast (SI, Figure S11). RCY, A_m and RCP were determined according to Herth et al.[28] Synthesis of precursor and reference compounds is described in Shalgunov et al.[21]

TCO-Modification Does Not Compromise BSmAB Integrity. We based our pretargeting vector on a Roche-developed, a fully human IgG1 monoclonal antibody with high binding affinity for fibrillar Aβ.[29,30] To enable BBB transport, we engineered a bispecific variant by fusing this antibody to a single-chain Fab fragment of the mouse transferrin receptor 1 (mTfR1)-binding antibody 8D3 (Figure 2A). The resulting bispecific antibody (hereafter referred to as BS-mAb) is designed to bind mTfR1 in a monovalent fashion. Monovalent engagement of TfR1 has been shown to enhance transcytosis across the blood−brain barrier, likely by reducing routing to lysosomal degradation pathways.[31] In contrast, bivalent binding can induce receptor clustering and promote lysosomal degradation of the TfR1−antibody complex, especially at higher antibody doses.[32] This feature is particularly important for brain pretargeting approaches, which require high doses of the TCO-bearing vector to achieve sufficient intracerebral concentrations for efficient ligation of the ^{18}F-labeled imaging agent. Thus, monovalent TfR1 binding is a key design consideration for ensuring effective delivery across the BBB.

TCO-functionalization of the BS-mAb was successfully performed through random conjugation to surface-exposed lysine residues using 5, 10, and 20 mol equiv of an NHS-TCO. Active TCO loadings of 3.7, 5.4, and 10.8 were obtained using a previously described procedure (Figure 2A).[33] The TCO construct used in this study has demonstrated improved *in vivo* stability, remaining active for over 3 days in similar molecular contexts, by resisting trans-to-cis isomerization.[33] This is important because the cis-isomer is no longer reactive in *in vivo* click chemistry applications. The enhanced stability arises from the use of a short linker between the mAb and the TCO moiety, which appears to hinder copper-containing enzymes from catalyzing the isomerization of TCO to its inactive cis-form.[33] This prolonged *in vivo* stability should provide a sufficient time window for the BS-mAb to reach and accumulate at the brain target site while clearing from the bloodstream, thereby enabling a high target-to-background ratio for effective brain PET imaging.

To further evaluate the impact of TCO-functionalization, we investigated the relationship between the TCO-functionalization and antibody integrity. These experiments showed that the BS-mAb could tolerate a relatively high active TCO load, up to approximately 10 active TCOs per antibody, without compromising structural integrity and binding affinities, as confirmed by size-exclusion chromatography (SEC) and

https://doi.org/10.1021/acs.molpharmaceut.5c01180
Mol. Pharmaceutics 2025, 22, 7600−7610

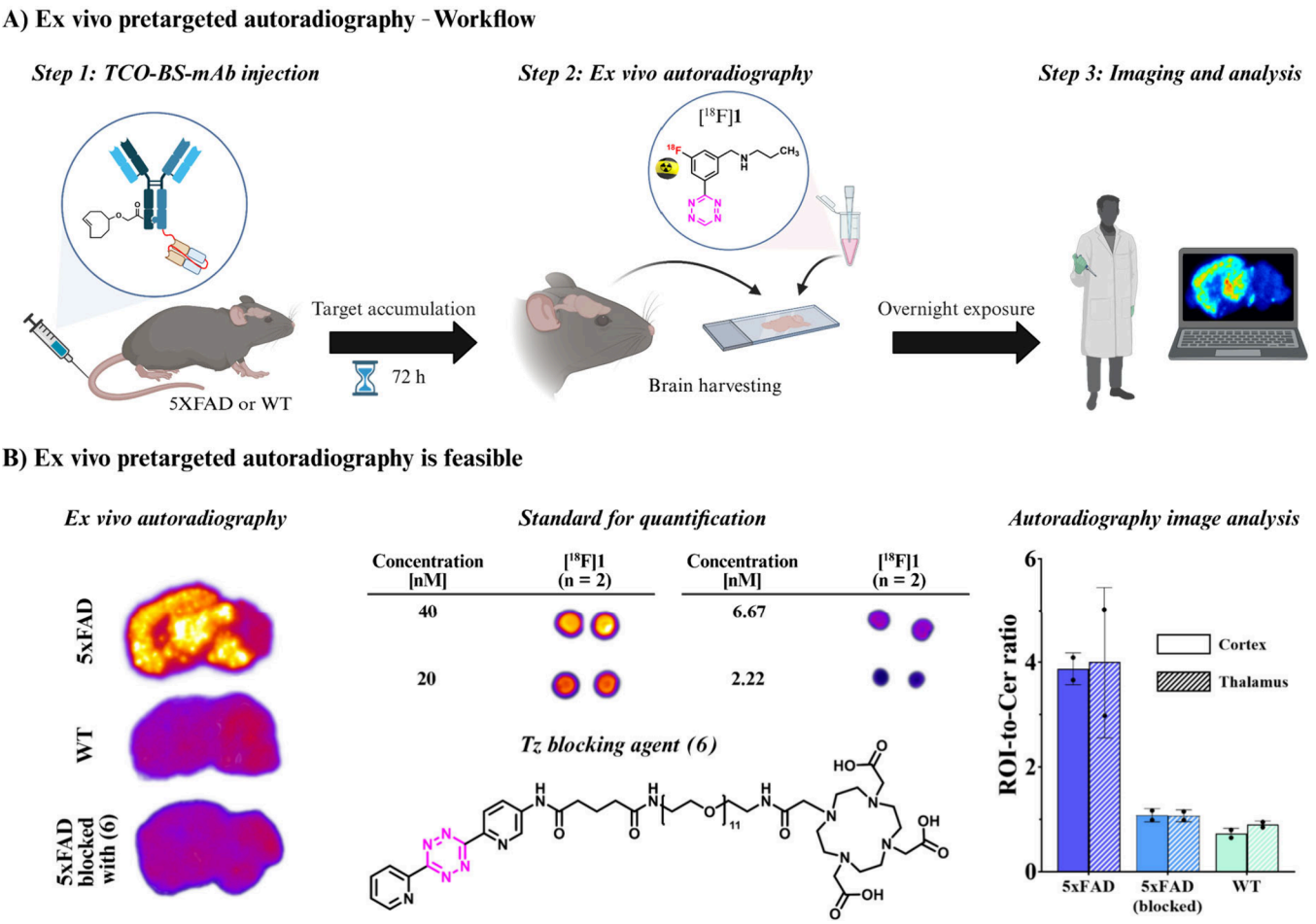

Figure 3. Specific brain binding of TCO-BS-mAb revealed by *ex vivo* pretargeted autoradiography. (A) Experimental workflow for *ex vivo* pretargeted autoradiography. 7.5-month-old 5xFAD (n = 2) and wild-type (WT, n = 2) mice were intravenously injected with TCO-BS-mAb (8 mg/kg). After 72 h, brains were extracted, sectioned, and incubated with 20 nM [^{18}F]**1**. Sections were then analyzed by autoradiography to assess *in situ* TCO−Tz ligation. (B) Representative autoradiograms of brain sections from a 5xFAD mouse (top left), a WT mouse (middle left), and a 5xFAD mouse pretreated with a blocking Tz (bottom left), all incubated with 20 nM [^{18}F]**1**. Increased radiotracer uptake is observed in the cortex and thalamus of the 5xFAD brain compared to WT and blocked controls. Radioactive standards used for quantification are shown (top middle), along with the blocking agent used in the control condition (bottom middle). Quantification of regional binding is shown on the right, expressed as cortex-to-cerebellum (Ctx/Cer) and thalamus-to-cerebellum (Thl/Cer) ratios. Error bars represent standard deviation (n = 2 per group). Abbreviations: Ctx, cortex; Thl, thalamus; Cer, cerebellum.

enzyme-linked immunosorbent assay (ELISA) (Figure 2B). Importantly, TCO conjugation had only a minor effect on the Aβ binding affinity, while mTfR1 binding remained unaffected (Figure 2B). The slight reduction in Aβ binding is likely due to steric hindrance caused by TCO modification at surface-exposed lysine residues near the antigen-binding regions and is more pronounced at higher TCO loads. Therefore, we chose not to exceed a TCO load of 10 per BS-mAb, as further increases would likely compromise Aβ binding affinity. Notably, similar TCO loading levels have been successfully used in tumor pretargeting strategies,[34] supporting the feasibility of using this TCO-BS-mAb for pretargeted brain imaging.

Retention of Click Reactivity of TCO-BS-mAb Following TfR1-Mediated Transcytosis. We next evaluated whether TCO groups remain reactive within brain tissue following intravenous (IV) administration of the TCO-BS-mAb. This analysis was performed after the antibody crossed the BBB via TfR1−mediated transcytosis, a process involving endosomal trafficking, during which the acidic environment could potentially compromise TCO reactivity.[33] For this study, we used transgenic 5xFAD mice that express human Aβ and presenilin-1 under the control of the Thy1 promoter, leading to robust and widespread Aβ expression in the brain. This model exhibits rapid and aggressive Aβ plaque formation, beginning as early as two months of age and progressing over time. The cortex and hippocampus are most severely affected, with moderate pathology in the thalamus and brainstem.[35,36] In contrast, the cerebellum remains largely unaffected by Aβ deposition, making it a reliable reference region for pretargeted Aβ PET imaging in this model.[37] To assess the stability and bioorthogonal reactivity of TCOs *in vivo*, 7.5-month-old 5xFAD and WT mice were intravenously administered TCO-BS-mAb at a dose of 5 nmol/kg (1 mg/kg). After 72 h, the brains were harvested, sectioned, and incubated with 0.3−20 nM [^{18}F]**1**. Autoradiographic analysis was then performed to visualize tracer ligation (Figure 3A). This *ex vivo* pretargeted autoradiography followed a protocol similar to our previously reported *in vitro* approach.[22,38] Autoradiographic analysis of brain tissue sections from 5xFAD mice incubated with 20 nM [^{18}F]**1** revealed a marked increase in signal intensity in Aβ-rich regions, including the cortex, hippocampus, thalamus, and

https://doi.org/10.1021/acs.molpharmaceut.5c01180
Mol. Pharmaceutics 2025, 22, 7600−7610

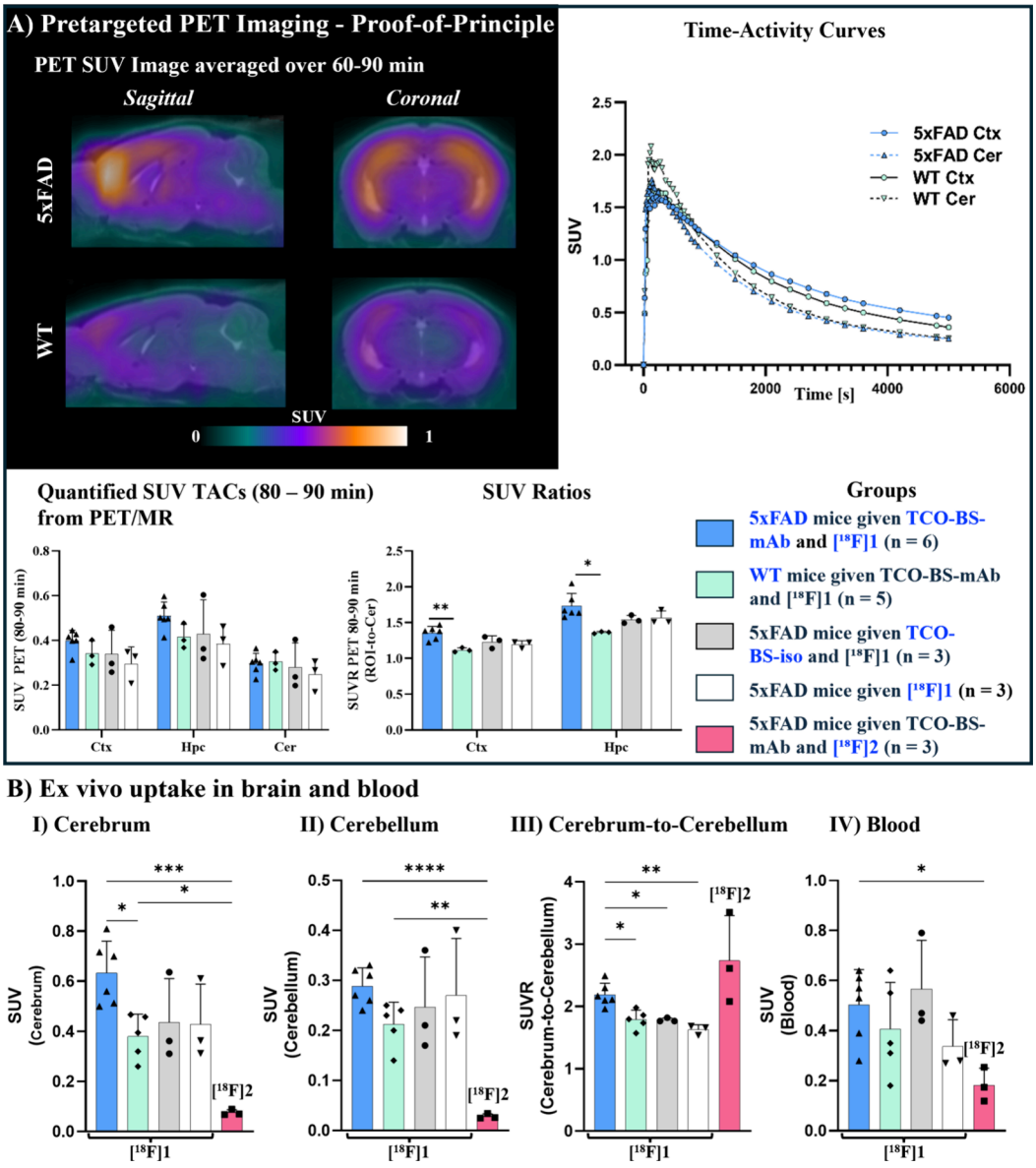

Figure 4. Brain pretargeting. (A) Representative sagittal and coronal pretargeted PET/CT images (averaged 60−90 min postinjection) of 5xFAD and WT mice pretreated with TCO-BS-mAb 3 days prior to administration of [^{18}F]**1**. Data are expressed as SUVs and coregistered on a mouse brain MRI reference template. Upper left panels: Visualized PET brain images. Upper right: TACs of SUV in the cortex and cerebellum, presented as interpolated means (n = 3). Lower left: Quantified SUV TACs (80−90 min) from PET/MR scans of 5xFAD and WT mice receiving TCO-BS-mAb or control TCO-BS-iso, followed by [^{18}F]**1**, or [^{18}F]**1** alone. Lower middle: SUV ratios (SUVR) were calculated as cortex-to-cerebellum and hippocampus-to-cerebellum ratios. (B) *Ex vivo* tissue analysis of [^{18}F]**1** and [^{18}F]**2** retention, expressed as SUV, in (I) cerebrum, (II) cerebellum, and (IV) blood; (III) *Ex vivo* cerebrum-to-cerebellum SUV ratios. *Ex vivo* SUV is defined as the ratio of radioactivity per gram of tissue to radioactivity per gram of body weight. Experimental groups: Blue, 5xFAD mice receiving TCO-BS-mAb and [^{18}F]**1** (n = 6); Teal, WT mice receiving TCO-BS-mAb and [^{18}F]**1** (n = 5); Gray, 5xFAD mice receiving TCO-BS-iso and [^{18}F]**1** (n = 3); White, 5xFAD mice receiving [^{18}F]**1**alone (n = 3); Pink, 5xFAD mice receiving TCO-BS-mAb and [^{18}F]**2** (n = 3). Abbreviations: Ctx, cortex; Hpc, hippocampus; Cer, cerebellum. Values are expressed as the mean ± standard deviation. Statistical significance was assessed using Brown−Forsythe and Welch one-way ANOVA followed by Dunnett's multiple comparisons test. Significance levels: $^{*}P \leq 0.05$, $^{**}P \leq 0.01$, $^{***}P \leq 0.001$, $^{****}P \leq 0.0001$.

brain stem. In contrast, WT mice exhibited uniformly low tracer uptake with no region-specific signal enhancement. Notably, cerebellar retention of [^{18}F]**1** was minimal and consistent between 5xFAD and WT mice (Figure 3B). Cortex- and thalamus-to-cerebellum uptake ratios reached approximately a value of 4 (Figure 3B), indicating highly specific ligation of [^{18}F]**1** and supporting its colocalization with Aβ pathology via TCO-Tz click reaction, with limited nonspecific binding. These results align with our previously published *in vitro* data using radiolabeled Tz for *in vitro* pretargeted autoradiography.[37,38]

To further confirm tracer specificity, a blocking study was conducted in which 5xFAD brain sections were preincubated with a 100-fold molar excess of a structurally unrelated Tz (**6**) (Figure 3B). This pretreatment abolished the region-specific retention of [^{18}F]**1** as evident from cortex- and thalamus-to-cerebellum ratios that were comparable to WT levels (Figure 3B). We assessed the impact of tracer concentration on autoradiographic performance by incubating 5xFAD sections

https://doi.org/10.1021/acs.molpharmaceut.5c01180
Mol. Pharmaceutics 2025, 22, 7600−7610

with lower concentrations of [^{18}F]**1** (1 and 0.3 nM) to better mimic *in vivo* conditions. Despite a decrease in absolute signal intensity, the distribution pattern remained consistent with that observed at 20 nM, showing preferential uptake in Aβ-rich regions. Importantly, the cortex- and thalamus-to-cerebellum ratios were preserved, further confirming the robustness of [^{18}F]**1** ligation even at subnanomolar levels.

Together, these findings indicate that TCO functionalization does not impair the *in vivo* performance of BS-mAb, as evidenced by effective BBB transcytosis and specific binding to Aβ pathology. Additionally, tissue-resident TCO remained reactive for at least 3 days postinjection, sufficient time to achieve high-contrast PET imaging. The blocking studies underscore the specificity of [^{18}F]**1**, as no binding was observed in the presence of competing Tz. Furthermore, the ability of [^{18}F]**1** to detect TCO at low concentrations highlights its promise for pretargeted PET imaging in the brain.

Brain Pretargeted ImmunoPET Imaging is Possible. Pretargeted brain PET imaging was conducted in female 5xFAD mice (n = 19) and age-matched female WT controls (n = 5). Mice received approximately 8 mg/kg TCO-BS-mAb, a TCO-functionalized isotype control (TCO-BS-iso), or radiolabeled Tz ([^{18}F]**1** or [^{18}F]**2**) without prior TCO-mAb administration. Intracerebral TCO ligation of [^{18}F]**1** and [^{18}F]**2** was evaluated through dynamic PET scans over 90 min, performed using small-animal PET/CT or PET/MR scanners (see Table 1 for detailed dosing information). Immediately following the scans, blood and brain tissues were collected. Brains were bisected along the midline: one hemisphere was processed for *ex vivo* autoradiography and histological analysis, while the other was dissected into the cerebrum and cerebellum for quantification of radiotracer uptake.

Pilot Study: Pretargeted PET Detects Brain Aβ in 5xFAD Mice. In a pilot pretargeted PET study, intracerebral [^{18}F]**1** ligation was evaluated in 5.5 month old 5xFAD mice (n = 2) and age-matched WT controls (n = 2), following administration of TCO-BS-mAb 3 days prior to imaging. PET scans revealed significantly higher retention of [^{18}F]**1** in Aβ-rich brain regions, particularly the cortex and hippocampus, of 5xFAD mice compared to WT animals, whereas tracer uptake in the cerebellum remained similar across both groups (Figure 4A). Time-activity curves (TACs) showed rapid initial tracer uptake in the brain, with peak standardized uptake values (C_{max}) of ∼1.8−2.2 SUV after 1−2 min postinjection, followed by a moderate brain washout phase. In 5xFAD mice, TACs progressively diverged from those of WT controls, with sustained elevations in Aβ-rich regions at later time points. In contrast, cerebellar retention remained comparable between the two groups throughout the imaging period (Figure 4B). These initial findings indicate that the administered dose and TCO loading were sufficient to enable the detection of brain-localized TCO-BS-mAb, supporting further expansion of the study.

Selecting the Best Tetrazine for Brain Pretargeted ImmunoPET Imaging. In our previous study, [^{18}F]**2** resulted in the best relative imaging contrast, whereas [^{18}F]**1** resulted in the best absolute imaging contrast.[21] Therefore, we decided to also evaluate [^{18}F]**2** in this study. Pretargeted PET imaging with [^{18}F]**2** showed minimal tracer retention in the brain (SI, Figure S8A), a finding confirmed by *ex vivo* analysis of cerebral, cerebellar, and blood tissues (Figure 4B). These results contrast with previous studies in rats, where intracerebral injection of a TCO-polymer followed by [^{18}F]**2** administration led to rapid, albeit low, brain uptake and fast clearance, producing high-contrast PET images.[21] The key difference between the two studies lies in the available TCO concentration: while the polymer approach provided an estimated TCO concentration of only ∼92 μM in an area of ∼40 μL,[21] it was estimated that only an average concentration of ∼0.092 μM was available in the whole brain (∼330 μL). The calculation for the estimation is given in the Supporting Information. We speculate that the combination of low TCO availability and limited brain uptake of [^{18}F]**2** significantly limits its utility for pretargeted brain imaging when the targeting vector is administered intravenously.

To investigate the reduced brain uptake and reduced *in vivo* click efficiency of [^{18}F]**2**, we conducted a metabolic study using a rat liver microsome assay. Tz **2** was found to be metabolized relatively rapidly, with a biological half-life of 74.9 ± 18.6 min and an estimated intrinsic clearance rate of 4.77 ± 1.18 μL·min^{-1}·mg^{-1}. In comparison, Tz **1** showed significantly greater metabolic stability, with a half-life of 229.7 ± 143 min and a clearance rate of 1.87 ± 1.17 μL·min^{-1}·mg^{-1}. Metabolite analysis revealed that the primary metabolite of Tz **1** is a hydroxylated, more polar derivative that retains the integrity of the tetrazine core, thereby preserving its ability to undergo click reactions. In contrast, the main metabolite of Tz **2** is a dihydro-tetrazine derivative, which disrupts the core structure and abolishes its click reactivity.[39] This finding can partly explain the reduced brain uptake and reduced *in vivo* click efficiency of [^{18}F]**2**. The findings also underscore several key requirements for successful *in vivo* click chemistry within the brain: (1) adequate numbers of TCO within the brain, (2) a Tz derivative with sufficient brain penetration, and (3) the metabolic stability of the Tz core to preserve its reactivity and enable effective *in vivo* ligation.

Confirmatory Study: Brain Pretargeted Immuno-PET Shows Target Binding. Due to the favorable *in vivo* performance of [^{18}F]**1** compared to [^{18}F]**2**, we selected [^{18}F]**1** as our lead candidate for further evaluation. To validate the findings from our pilot study, we expanded the experimental design by increasing the sample size and incorporating additional control groups. In this new, second cohort, PET pretargeted imaging with [^{18}F]**1** reproduced the brain uptake and regional distribution patterns observed in the pilot study (Figure 4). Increased intragroup variability was noted across all experimental groups, evident in (1) averaged PET data (60−90 min; SI, Figure S8B), (2) quantified cortical, hippocampal, and cerebellar time-activity curves (TACs) (80−90 min; Figure 4A), and (3) *ex vivo* tracer quantification (Figure 4B). The source of this variability remains unclear; however, individual differences in the expression of BBB efflux transporters, such as P-glycoprotein 1, or in metabolic enzyme activity may contribute to the observed effects. Notably, variability was substantially reduced when analyzing standard uptake value (SUV) ratios, specifically cortex-to-cerebellum ($SUVR_{Ctx/Cer}$) and hippocampus-to-cerebellum ($SUVR_{Hpc/Cer}$), derived from extracted TACs. In 5xFAD mice, $SUVR_{Ctx/Cer}$ and $SUVR_{Hpc/Cer}$ were elevated by 22% ($t(6.63) = 5.75$, $p = 0.0037$, Dunnett's T3 multiple comparisons test) and 27% ($t(5.12) = 5.11$, $p = 0.0173$, Dunnett's T3 multiple comparisons test), respectively, compared to WT mice. Control groups receiving BS-iso with [^{18}F]**1** or [^{18}F]**1** alone exhibited a slight increase in SUVRs compared to that in WT mice, though differences were not statistically significant

https://doi.org/10.1021/acs.molpharmaceut.5c01180
Mol. Pharmaceutics 2025, 22, 7600−7610

relative to either 5xFAD or WT mice pretreated with TCO-BS-mAb (Figure 4B).

To validate PET quantification, *ex vivo* biodistribution was performed immediately postimaging. Tracer uptake in brain and blood tissues mirrored the PET results, with cerebral [^{18}F]**1** retention in TCO-BS-mAb-treated 5xFAD mice being 67% higher than in WT mice ($t(8.82) = 3.88$, $p = 0.0308$, Dunnett's T3 multiple comparisons test; Figure 4B). A similar trend was observed compared to the control groups. Cerebellar uptake remained consistent across all groups (Figure 4B). *Ex vivo* determined cerebrum-to-cerebellum ratios further confirmed increased tracer accumulation in TCO-BS-mAb-treated 5xFAD mice, with elevations of 22.4% compared to WT mice ($t(9.00) = 3.94$, $p = 0.0282$, Dunnett's T3 multiple comparisons test), 22.7% compared to 5xFAD mice receiving BS-iso and [^{18}F]**1** ($t(5.52) = 5.21$, $p = 0.0148$, Dunnett's T3 multiple comparisons test), and 34.4% compared to 5xFAD mice receiving [^{18}F]**1** alone ($t(6.99) = 6.36$, $p = 0.0031$, Dunnett's T3 multiple comparisons test; Figure 4B).

Autoradiography and Histology Confirm PET Findings. Following PET imaging, we performed a detailed characterization of the spatial distribution of both the TCO-functionalized mAb and [^{18}F]**1** in the brains of 5xFAD and WT mice. The distribution of [^{18}F]**1** was assessed by *ex vivo* autoradiography, while the localization of the injected antibodies was visualized using antihuman IgG immunostaining (Figure 5). *Ex vivo* autoradiography of PET-imaged mice closely matched the patterns observed using *in vitro* autoradiography, with significantly increased tracer uptake in Aβ-rich brain regions of 5xFAD mice treated with TCO-BS-mAb.[37,38] In contrast, minimal tracer accumulation was detected in the same brain regions of WT mice and 5xFAD mice treated with either BS-iso or [^{18}F]**1** alone.

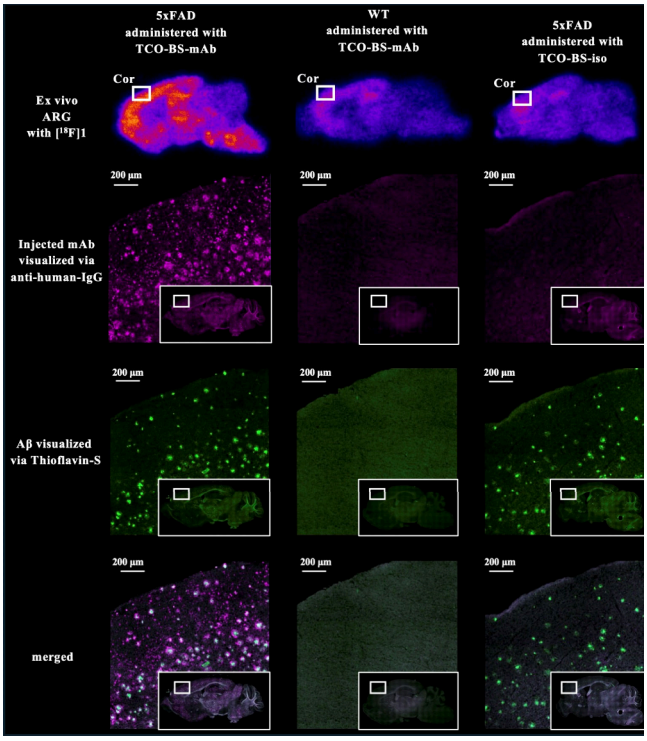

Figure 5. Post-mortem analysis of [^{18}F]**1** and TCO-mAb distribution in the brain following pretargeted PET imaging. Representative brain sections from 5xFAD and WT mice were injected with either TCO-BS-mAb or TCO-BS-iso, followed by administration of [^{18}F]**1**. Sections were analyzed via *ex vivo* autoradiography and fluorescent staining. Amyloid-β (Aβ) plaques were visualized using thioflavin S (green), while tissue-resident mAbs were detected using Alexa Fluor 568-conjugated goat antihuman IgG (purple).

Histological analysis of brain sections further validated these findings. In 5xFAD mice, colocalization of TCO-BS-mAb with Aβ plaques, visualized by thioflavin S staining, was observed and overlapped with regions of high [^{18}F]**1** retention. As expected, no antibody signal was detected in brain tissue sections from WT mice or from 5xFAD mice treated with BS-iso or [^{18}F]**1** alone, confirming the specificity of mAb localization.

Interestingly, the intragroup variability observed in PET and *ex vivo* biodistribution data was also apparent in autoradiographic images (SI, Figure S9), confirming the reproducibility of the individual [^{18}F]**1** uptake pattern across different experimental readouts and supporting the robustness of the overall methodology.

CONCLUSION

We report, for the first time, successful antibody-based pretargeting across the BBB using our novel, in-house-developed Tz, [^{18}F]**1**. In an Aβ mouse model, [^{18}F]**1** enabled specific detection of a TCO-functionalized bispecific antibody targeting both Aβ and mTfR by *in vivo* PET imaging. The PET signal was validated by *ex vivo* autoradiography and histological assessments. This work establishes the proof-of-concept for a versatile imaging platform for quantifying brain uptake and target binding based on pretargeted PET imaging, particularly for challenging CNS targets. The approach shows strong potential as a translational tool in both preclinical and clinical settings to support therapeutic development and monitoring of treatment monitoring. While demonstrated in the 5xFAD model, further evaluation in disease-relevant models is warranted. In particular, mAb dosing or lag time between Tz administration of mAb should be improved in order to achieve even better imaging contrast. Overall, this strategy marks a significant advance in noninvasive imaging of brain targets with potential to accelerate progress in CNS drug development.

ASSOCIATED CONTENT

Supporting Information

The Supporting Information is available free of charge at https://pubs.acs.org/doi/10.1021/acs.molpharmaceut.5c01180.

Additional experimental details including: metabolic stability, autoradiography studies, PET imaging, and *ex vivo* evaluation (PDF)

AUTHOR INFORMATION

Corresponding Authors

Matthias M. Herth − *Department of Drug Design and Pharmacology, Faculty of Health and Medical Sciences, University of Copenhagen, 2100 Copenhagen, Denmark; Department of Clinical Physiology, Nuclear Medicine & PET, Rigshospitalet, 2100 Copenhagen, Denmark;* orcid.org/0000-0002-7788-513X; Email: matthias.herth@sund.ku.dk

Umberto Maria Battisti − *Department of Drug Design and Pharmacology, Faculty of Health and Medical Sciences, University of Copenhagen, 2100 Copenhagen, Denmark;*

https://doi.org/10.1021/acs.molpharmaceut.5c01180
Mol. Pharmaceutics 2025, 22, 7600−7610

orcid.org/0000-0002-1012-8644;
Email: umberto.battisti@sund.ku.dk

Andreas Kjaer − *Cluster for Molecular Imaging, Department of Biomedical Sciences, University of Copenhagen, 2100 Copenhagen Ø, Denmark; Department of Clinical Physiology, Nuclear Medicine & PET, Rigshospitalet, 2100 Copenhagen, Denmark;* orcid.org/0000-0002-2706-5547;
Email: akjaer@sund.ku.dk

Authors

Tobias Gustavsson − *Department of Drug Design and Pharmacology, Faculty of Health and Medical Sciences, University of Copenhagen, 2100 Copenhagen, Denmark*

Thomas Kustermann − *Pharma Research and Early Development, Roche Innovation Center Basel, F. Hoffmann-La Roche Ltd, CH-4070 Basel, Switzerland*

Lars Hvass − *Cluster for Molecular Imaging, Department of Biomedical Sciences, University of Copenhagen, 2100 Copenhagen Ø, Denmark; Department of Clinical Physiology, Nuclear Medicine & PET, Rigshospitalet, 2100 Copenhagen, Denmark;* orcid.org/0000-0003-2048-2409

Thomas E. Wuensche − *Department of Drug Design and Pharmacology, Faculty of Health and Medical Sciences, University of Copenhagen, 2100 Copenhagen, Denmark*

Anne Skovsbo Clausen − *Cluster for Molecular Imaging, Department of Biomedical Sciences, University of Copenhagen, 2100 Copenhagen Ø, Denmark; Department of Clinical Physiology, Nuclear Medicine & PET, Rigshospitalet, 2100 Copenhagen, Denmark*

Sophie Stotz − *Department of Drug Design and Pharmacology, Faculty of Health and Medical Sciences, University of Copenhagen, 2100 Copenhagen, Denmark;* orcid.org/0000-0003-4020-1088

Vladimir Shalgunov − *Department of Clinical Physiology, Nuclear Medicine & PET, Rigshospitalet, 2100 Copenhagen, Denmark;* orcid.org/0000-0001-8956-1207

Sara Lopes van den Broek − *Department of Drug Design and Pharmacology, Faculty of Health and Medical Sciences, University of Copenhagen, 2100 Copenhagen, Denmark*

Gitte M. Knudsen − *Neurobiology Research Unit and Institute for Clinical Medicine, Copenhagen University Hospital Rigshospitalet and University of Copenhagen, DK-2100 Copenhagen, Denmark*

Blanca Aldana − *Department of Drug Design and Pharmacology, Faculty of Health and Medical Sciences, University of Copenhagen, 2100 Copenhagen, Denmark*

Elena Ferri − *Department of Life Sciences, University of Modena and Reggio Emilia, 41125 Modena, Italy;* orcid.org/0009-0000-0360-8538

Giuseppe Cannazza − *Department of Life Sciences, University of Modena and Reggio Emilia, 41125 Modena, Italy;* orcid.org/0000-0002-7347-7315

Jens Niewoehner − *Pharma Research and Early Development, Roche Innovation Center Basel, F. Hoffmann-La Roche Ltd, CH-4070 Basel, Switzerland*

Luca Gobbi − *Pharma Research and Early Development, Roche Innovation Center Basel, F. Hoffmann-La Roche Ltd, CH-4070 Basel, Switzerland;* orcid.org/0000-0002-0563-2491

Michael Honer − *Pharma Research and Early Development, Roche Innovation Center Basel, F. Hoffmann-La Roche Ltd, CH-4070 Basel, Switzerland*

Complete contact information is available at: https://pubs.acs.org/10.1021/acs.molpharmaceut.5c01180

Author Contributions

TG, TK, and LH contributed equally; TB, TK, GMK, BA, LG, MH, UMB, AK and MMH designed the project; JN generated the bispecific antibody. TCO-conjugation and *in vitro* evaluation was performed by TB, TEW, ST and SLB. Animal experiments were conducted by TB, LH, ASC and ST. Tetrazine precursors were synthesized by UMB. Labeling was conducted by VS, TEW and TB. ST, TB and LH processed and quantified the PET scans. TB, LH, TEW and ST analyzed the data. EF and GC carried out the metabolism study. TB, TK, TEW, UMB, AK and MMH have written the manuscript with input from LH, ST, GMK, BA, LG and MH

Notes

Ethical Statement: All animal procedures were performed in accordance with the European Commission's Directive 2010/63/EU for animal research and approved by the Danish Council for Animal Ethics together with the Department of Experimental Medicine, University of Copenhagen, License number: 2023-15-0201-01362.

The authors declare the following competing financial interest(s): AK and MMH are the founders of PreTT ApS, a company that has licensed the patent WO2020108720A1 from the University of Copenhagen, which was applied in this study; both AK and MMH are listed as inventors on this patent.

■ ACKNOWLEDGMENTS

This project has received funding from the European Union's EU Framework Programme for Research and Innovation Horizon 2020, under grant agreement nos. 668532 and 670261. It also received funding from the European Union's Horizon research and innovation programme under the Marie Skłodowska-Curie grant agreement no. 101110589. SS was supported by BRIDGE−Translational Excellence Programme at the Faculty of Health and Medical Sciences, University of Copenhagen, funded by the Novo Nordisk Foundation (grant agreement no. NNF23SA0087869). GMK and MMH have received funding from the Novo Tandem Programme, supported by the Novo Nordisk Foundation (grant agreement no. NNF23OC0082288). Finally, the Research Council for Independent Research (grant agreement no. 8022-00187B) is acknowledged. AK has received funding from the Lundbeck Foundation, the Novo Nordisk Foundation, the Innovation Fund Denmark, the Danish Cancer Society, the Research Foundation of Rigshospitalet, Andreas Kjaer is a Lundbeck Foundation Professor.

■ REFERENCES

(1) Pardridge, W. M. The blood-brain barrier: Bottleneck in brain drug development. *NeuroRX* **2005**, *2*, 3−14.

(2) Pemberton, H. G.; et al. Quantification of amyloid PET for future clinical use: a state-of-the-art review. *Eur. J. Nucl. Med. Mol. Imaging* **2022**, *49*, 3508−3528.

(3) Groot, C.; Villeneuve, S.; Smith, R.; Hansson, O.; Ossenkoppele, R. Tau PET Imaging in Neurodegenerative Disorders. *J. Nucl. Med.* **2022**, *63*, 20S−26S.

(4) Hultqvist, G.; Syvänen, S.; Fang, X. T.; Lannfelt, L.; Sehlin, D. Bivalent brain shuttle increases antibody uptake by monovalent binding to the transferrin receptor. *Theranostics* **2017**, *7*, 308−318.

(5) Pardridge, W. M. Drug Transport across the Blood−Brain Barrier. *Journal of Cerebral Blood Flow & Metabolism* **2012**, *32*, 1959−1972.

(6) Syvänen, S.; et al. Fluorine-18-Labeled Antibody Ligands for PET Imaging of Amyloid-β in Brain. *ACS Chem. Neurosci.* **2020**, *11*, 4460−4468.
(7) Sehlin, D.; Fang, X. T.; Meier, S. R.; Jansson, M.; Syvänen, S. Pharmacokinetics, biodistribution and brain retention of a bispecific antibody-based PET radioligand for imaging of amyloid-β. *Sci. Rep* **2017**, *7*, 17254.
(8) Wuensche, T. E.; et al. Advancing 89Zr-immuno-PET in neuroscience with a bispecific anti-amyloid-beta monoclonal antibody − the choice of chelator is essential. *Theranostics* **2022**, *12*, 7067−7079.
(9) Sehlin, D.; Fang, X. T.; Cato, L.; Antoni, G.; Lannfelt, L.; Syvanen, S. Antibody-based PET imaging of amyloid beta in mouse models of Alzheimer's disease. *Nat. Commun.* **2016**, *7*, 10759.
(10) Roshanbin, S.; Xiong, M.; Hultqvist, G.; Soderberg, L.; Zachrisson, O.; Meier, S.; Ekmark-Lewen, S.; Bergstrom, J.; Ingelsson, M.; Sehlin, D.; Syvanen, S. In vivo imaging of alpha-synuclein with antibody-based PET. *Neuropharmacology* **2022**, *208*, 108985.
(11) Shojaei, M.; et al. PET imaging of microglia in Alzheimer's disease using copper-64 labeled TREM2 antibodies. *Theranostics* **2024**, *14*, 6319−6336.
(12) Stergiou, N.; et al. Application of 89Zr-DFO*-immuno-PET to assess improved target engagement of a bispecific anti-amyloid-ß monoclonal antibody. *Eur. J. Nucl. Med. Mol. Imaging* **2023**, *50*, 1306−1317.
(13) Altai, M.; Membreno, R.; Cook, B.; Tolmachev, V.; Zeglis, B. M. Pretargeted Imaging and Therapy. *J. Nucl. Med.* **2017**, *58*, 1553−1559.
(14) Stéen, E. J. L.; et al. Pretargeting in nuclear imaging and radionuclide therapy: Improving efficacy of theranostics and nanomedicines. *Biomaterials* **2018**, *179*, 209−245.
(15) Scinto, S. L.; Bilodeau, D. A.; Hincapie, R.; Lee, W.; Nguyen, S. S.; Xu, M.; am Ende, C. W.; Finn, M. G.; Lang, K.; Lin, Q.; Pezacki, J. P.; Prescher, J. A.; Robillard, M. S.; Fox, J. M.; et al. Bioorthogonal chemistry. *Nature Reviews Methods Primers* **2021**, *1*, 30.
(16) Bird, R. E.; Lemmel, S. A.; Yu, X.; Zhou, Q. A. Bioorthogonal Chemistry and Its Applications. *Bioconjugate Chem.* **2021**, *32*, 2457−2479.
(17) García-Vázquez, R.; Battisti, U.; Herth, M. Recent Advances in the Development of Tetrazine Ligation Tools for Pretargeted Nuclear Imaging. *Pharmaceuticals* **2022**, *15*, 685.
(18) Edelmann, M. R.; et al. Evaluation of Tetrazine Tracers for Pretargeted Imaging within the Central Nervous System. *Bioconjug Chem.* **2023**, *34*, 1882−1893.
(19) Oliveira, B. L.; Guo, Z.; Bernardes, G. J. L. Inverse electron demand Diels−Alder reactions in chemical biology. *Chem. Soc. Rev.* **2017**, *46*, 4895−4950.
(20) Cook, B. E.; et al. Non-invasive Imaging of Antisense Oligonucleotides in the Brain via In Vivo Click Chemistry. *Mol. Imaging Biol.* **2022**, *24*, 940−949.
(21) Shalgunov, V.; et al. Pretargeted imaging beyond the blood-brain barrier. *RSC Med. Chem.* **2023**, *14*, 444−453.
(22) Bredack, C.; Edelmann, M. R.; Borroni, E.; Gobbi, L. C.; Honer, M. Antibody-Based In Vivo Imaging of Central Nervous System Targets—Evaluation of a Pretargeting Approach Utilizing a TCO-Conjugated Brain Shuttle Antibody and Radiolabeled Tetrazines. *Pharmaceuticals* **2022**, *15*, 1445.
(23) Shalgunov, V.; van den Broek, S. L.; Andersen, I. V.; Raval, N. R.; Schafer, G.; Barz, M.; Herth, M. M.; Battisti, U. M. Evaluation of F-537-Tetrazine in a model for brain pretargeting imaging. Comparison to N-(3-[18F] fluoro-5-(1,2,4,5-tetrazin-3-yl)benzyl)-propan-1-amine. *Nucl. Med. Biol.* **2024**, *128−129*, 108877.
(24) Schlein, E.; Rokka, J.; Odell, L. R.; van den Broek, S. L.; Herth, M. M.; Battisti, U. M.; Syvanen, S.; Sehlin, D.; Eriksson, J. Synthesis and evaluation of fluorine-18 labelled tetrazines as pre-targeting imaging agents for PET. *EJNMMI Radiopharm Chem.* **2024**, *9*, 21.
(25) Mirrione, M. M.; et al. A novel approach for imaging brain−behavior relationships in mice reveals unexpected metabolic patterns during seizures in the absence of tissue plasminogen activator. *Neuroimage* **2007**, *38*, 34−42.
(26) Presotto, L.; Bettinardi, V.; Mercatelli, D.; Picchio, M.; Morari, M.; Moresco, R. M.; Belloli, S.; et al. Development of a new toolbox for mouse PET−CT brain image analysis fully based on CT images and validation in a PD mouse model. *Sci. Rep* **2022**, *12*, 15822.
(27) García-Vázquez, R.; et al. Direct Cu-mediated aromatic ^{18}F-labeling of highly reactive tetrazines for pretargeted bioorthogonal PET imaging. *Chem. Sci.* **2021**, *12*, 11668−11675.
(28) Herth, M. M.; et al. On the consensus nomenclature rules for radiopharmaceutical chemistry − Reconsideration of radiochemical conversion. *Nucl. Med. Biol.* **2021**, *93*, 19−21.
(29) Bohrmann, B.; Baumann, K.; Benz, J.; Gerber, F.; Huber, W.; Knoflach, F.; Messer, J.; Oroszlan, K.; Rauchenberger, R.; Richter, W. F.; Rothe, C.; Urban, M.; Bardroff, M.; Winter, M.; Nordstedt, C.; Loetscher, H.; et al. Gantenerumab: A Novel Human Anti-Aβ Antibody Demonstrates Sustained Cerebral Amyloid-β Binding and Elicits Cell-Mediated Removal of Human Amyloid-β. *Journal of Alzheimer's Disease* **2012**, *28*, 49−69.
(30) Söderberg, L.; et al. Lecanemab, Aducanumab, and Gantenerumab — Binding Profiles to Different Forms of Amyloid-Beta Might Explain Efficacy and Side Effects in Clinical Trials for Alzheimer's Disease. *Neurotherapeutics* **2023**, *20*, 195−206.
(31) Niewoehner, J.; et al. Increased Brain Penetration and Potency of a Therapeutic Antibody Using a Monovalent Molecular Shuttle. *Neuron* **2014**, *81*, 49−60.
(32) Morrison, J. I.; Metzendorf, N. G.; Rofo, F.; Petrovic, A.; Hultqvist, G. A single-chain fragment constant design enables easy production of a monovalent blood−brain barrier transporter and provides an improved brain uptake at elevated doses. *J. Neurochem* **2023**, *165*, 413−425.
(33) Rossin, R.; et al. Highly Reactive *trans* -Cyclooctene Tags with Improved Stability for Diels−Alder Chemistry in Living Systems. *Bioconjug Chem.* **2013**, *24*, 1210−1217.
(34) Rossin, R.; et al. In Vivo Chemistry for Pretargeted Tumor Imaging in Live Mice. *Angew. Chem., Int. Ed.* **2010**, *49*, 3375−3378.
(35) Oakley, H.; et al. Intraneuronal β-Amyloid Aggregates, Neurodegeneration, and Neuron Loss in Transgenic Mice with Five Familial Alzheimer's Disease Mutations: Potential Factors in Amyloid Plaque Formation. *J. Neurosci.* **2006**, *26*, 10129−10140.
(36) Forner, S.; Kawauchi, S.; Balderrama-Gutierrez, G.; Kramar, E. A.; Matheos, D. P.; Phan, J.; Javonillo, D. I.; Tran, K. M.; Hingco, E.; da Cunha, C.; Rezaie, N.; Alcantara, J. A.; Baglietto-Vargas, D.; Jansen, C.; Neumann, J.; Wood, M. A.; MacGregor, G. R.; Mortazavi, A.; Tenner, A. J.; LaFerla, F. M.; Green, K. N. Systematic phenotyping and characterization of the 5xFAD mouse model of Alzheimer's disease. *Sci. Data* **2021**, *8*, 270.
(37) Lopes van den Broek, S.; Sehlin, D.; Andersen, J. V.; Aldana, B. I.; Beschorner, N.; Nedergaard, M.; Knudsen, G. M.; Syvanen, S.; Herth, M. M. The Alzheimer's disease 5xFAD mouse model is best suited to investigate pretargeted imaging approaches beyond the blood-brain barrier. *Frontiers in Nuclear Medicine* **2022**, *2*, 1001722.
(38) Lopes van den Broek, S.; Shalgunov, V.; Garcia Vazquez, R.; Beschorner, N.; Bidesi, N. S. R.; Nedergaard, M.; Knudsen, G. M.; Sehlin, D.; Syvanen, S.; Herth, M. M. Pretargeted Imaging beyond the Blood−Brain Barrier—Utopia or Feasible? *Pharmaceuticals* **2022**, *15*, 1191.
(39) Otaru, S.; Niemikoski, H.; Sarparanta, M.; Airaksinen, A. J. Metabolism of a Bioorthogonal PET Tracer Candidate [^{19}F/^{18}F]SiFA-Tetrazine in Mouse Liver Microsomes: Biotransformation Pathways and Defluorination Investigated by UHPLC-HRMS. *Mol. Pharmaceutics* **2020**, *17*, 3106−3115.

https://doi.org/10.1021/acs.molpharmaceut.5c01180
Mol. Pharmaceutics 2025, 22, 7600−7610